The High Performance of 4H-SiC for the Photodetector in High-speed Optocoupler

Tian Lei[1], Qi Zhang[1], Yi Jiang[2], Yu He[3], and Hang Mao[3]

[1]Xi'an University of Posts and Telecommunications
[2]Shaanxi Key Laboratory for Theoretical Physics Frontiers
[3]Electronic Engineering

September 23, 2022

Abstract

In this letter, a high-performance photodetector was established with the 4H-SiC structure for the high-speed optocoupler. It is found that the band gap of the doped 4H-SiC is reduced, where the electrons can transmit to the conduction band easier. It improves the photoelectric response speed and the light absorption rate of the system is effectively improved. Under the 840nm incident light, the transient response of the optocoupler are 210ns and 155ns, respectively. During the temperature changed, the maximum variation value is 12ns. The response speed of the whole chip is increased and it changed very little with the variation of the input photocurrent and the operation temperature.

The High Performance of 4H-SiC for the Photodetector in High-speed Optocoupler

L. Tian[1], Q. Zhang[1], Z.Y. Jiang[2], C.Y. He[1] and M.H. Mao[1]

[1] *School of Electronic Engineering, Xi'an University of Posts and Telecommunications, Xi'an 710121, China*

[2] Shaanxi Key Laboratory for Theoretical Physics Frontiers, Institute of Modern Physics, Northwest University, Xi'an 710127, China

Email: tianlei@xupt.edu.cn

In this letter, a high-performance photodetector was established with the 4H-SiC structure for the high-speed optocoupler. It is found that the band gap of the doped 4H-SiC is reduced, where the electrons can transmit to the conduction band easier. It improves the photoelectric response speed and the light absorption rate of the system is effectively improved. Under the 840nm incident light, the transient response of the optocoupler are 210ns and 155ns, respectively. During the temperature changed, the maximum variation value is 12ns. The response speed of the whole chip is increased and it changed very little with the variation of the input photocurrent and the operation temperature.

Introduction: High speed photodetector (PD) in the optocoupler has become more and more important in the complicated industry control and power network [1]. Traditionally the Silicon material was used in the first high-speed optocoupler [2]. The main concern is cut down the transit time, then the rise time and fall time of this optocoupler are around 0.5μs. However, the influences of the response speed of the photodetector is not analyzed in details, especially in the construction of them. When the optocoupler worked in the high-speed environment, the post stage required more higher response speed of the photodetector. In the industry, the usual solution to short the response time is only through adjust the ratio of the width and length of the MOSFET arrays. This method could change the response speed slightly, but it could not short the response time fundamentally. A comparative study was made between different materials of the

photodetector structures [3]. Although the new material was used, the response time of the whole chip is limited in 0.74μs. With the thicker intrinsic region, the transit time of the carriers would become longer [4]. It will result in the delay of the response time of the whole chip. So, the research of the high-speed integrated photodetector is critical for the optocoupler [5].

In this Letter an n-type dopant in 4H-SiC in the PD structure was constructed to decrease the response time. And another benefit of the structure is to broaden the wavelength of the absorbed light. It ensures the stability of the input photocurrent (I_{ph}) [6].

Device fabrication: In the photodetector design, SiC is selected as the core material which will be used in the power network [7]. All the geometric optimizations and calculations were performed with the Vienna abinitio simulation package (VASP). The projector augmented wave (PAW) approach is used to describe the interaction between the core and valence electrons. The generalized gradient approximation of Perdew-Burke-Ernzerh of (PBE) was applied to describe the exchange correlation function. The valence electrons configurations considered in this study include C ($2s^2 2p^2$), Si ($3s^2 3p^2$) and P ($3s^2 3p^3$). The spin-polarization was considered in all calculations. We set the cutoff energy to be 450eV and a Monkhorst-Packmesh of 2×2×2 k-points to sample the two-dimensional Brilliouin zone for the geometry optimizations and electronic structure calculations [8-9]. All atoms were fully relaxed until the convergence criteria of energy and force were less than 1×10-5eV and 0.05 eV/Å, respectively. Considering that in general the PBE functional underestimates the band gaps of semiconductors, all electronic structures were calculated using the Heyd–Scuseria–Ernzerhof (HSE06) hybrid functional [10]. Fig 1 shows the illustration of the improved structure of the photodiode which constructed the PD and the photograph of the PD.

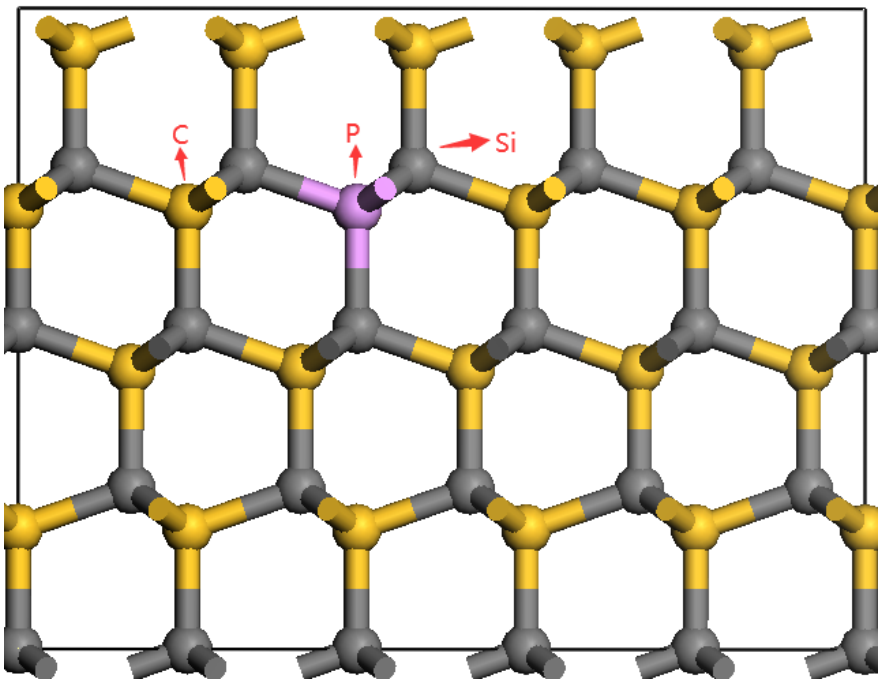

(a) Structure of the 4H-SiC

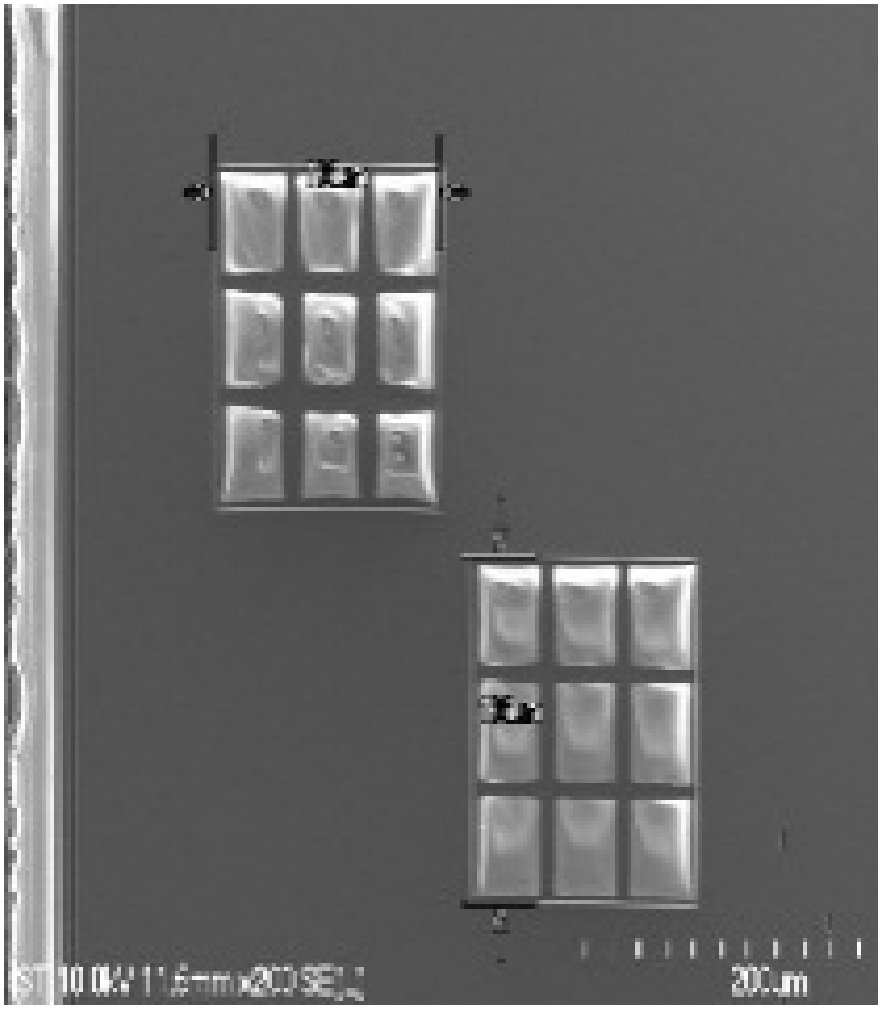

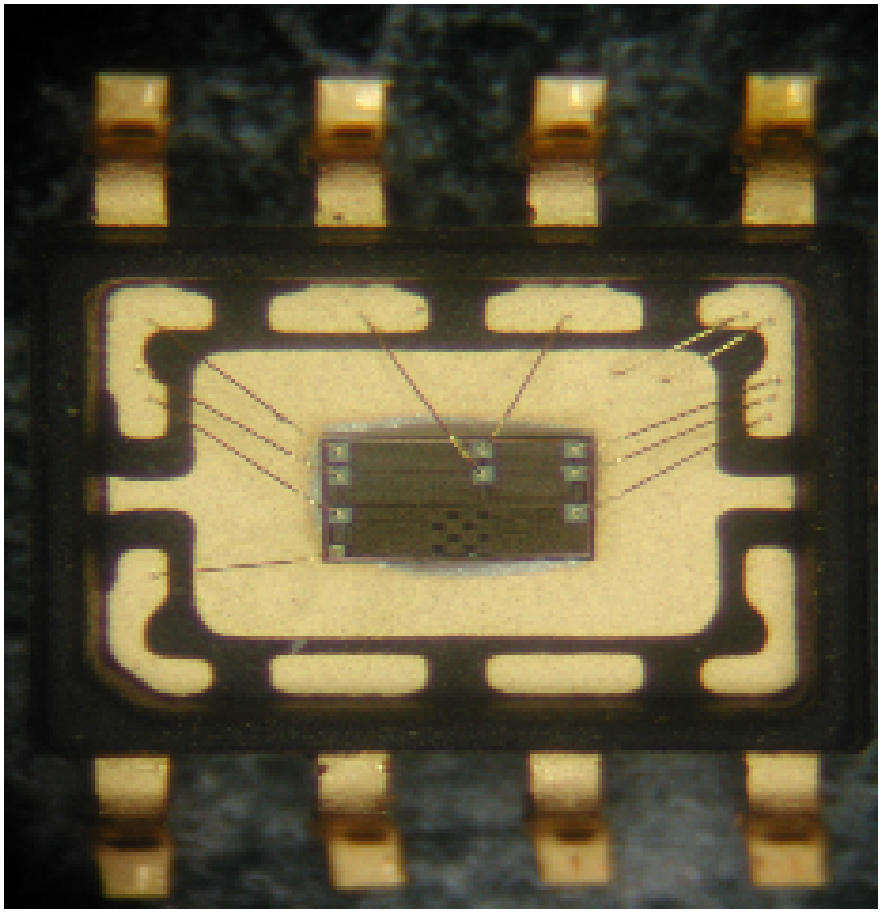

(b) Block of PD (c) Micrograph of the chip

Fig 1 *Structure and photograph of fabricated PD*

The geometry optimizations of 4H-SiC is shown in Fig 1(a). The space group of the 4H-SiC is P63m [11]. The optimized lattice constants of the monolayer 4H-SiC were a=b=1.5455Å, which were basically consistent with the experimental data (1.2324Å). According to the optimized structure of 4H-SiC, the PD was fabricated in Fig. 1 (b), which the inner-block was 45μm wide and 45μm long with two spacing of 10μm, and the active areas was 166*166μm^2. The micrograph of the whole chip is shown in Fig. 1(c), the die size is 1420*1310μm^2.

Design and simulation: The Phosphorus substitutes Si formation energy is -3.26eV, and the interstitial doping formation energy is 3.32eV. So, the interstitial doping is difficult to construct. Here, we choose the P substitute Si in the 4H-SiC structure.

Compared with the intrinsic SiC band, the P doping introduced the impurity energy level. The fermi level went into the CBM and the n type doping is constructed. The band structure of the SiC is showed in Fig. 2.

(a) Intrinsic (b) P substitute Si

Fig 2 *Band structures of 4H-SiC*

Fig. 2 shows the energy band structure with the high symmetry direction of the first Brillouin zone before and after 4H-SiC doping. Fig. 2(a) shows the top of the valence band of the intrinsic 4H-SiC is located at

the Γ point of the Brillouin zone, and the bottom of the conduction band is located at the M point of the Brillouin zone. It is an indirect bandgap semiconductor with a forbidden band width of 2.215 eV. Fig. 2(b) shows the energy band structures of 4H-SiC after P substitution of Si atoms. The doped P atom generates a donor energy level that can provide electrons near the bottom of the conduction band. It moves down the bottom of the conduction band and the top of the valence band, and the Fermi level enters the conduction band. The doped system forming n-type doping and the semiconductor occurs. The doping system increase the number of energy levels that electrons occupies and carrier concentration.

In order to clearly analyze the electronic structure of the doping system, the total density of states (TDOS) and the partial density of states (PDOS) were calculated for the 4H-SiC by the HSE06 functional and were plotted in Fig. 3. and the band gaps of the SiC is 2.215eV which basically consistent with experimental values.

Intrinsic (b) P substitute Si (c) P substitute C

Fig 3 *DOS of 4H-SiC*

Comparing with the intrinsic SiC, the band gap of the P doping structure was reduced, which increases the spectral absorption range. Since the doping atoms have a great influence on the DOS of the adjacent atoms, so the adjacent C atoms and Si atoms of the doping atom and the P atoms were compared. In Fig. 3(a), for intrinsic 4H-SiC, the top of the VBM is mainly composed of the Si-3p state and the C-2p state. The bottom of the CBM is mainly contributed by the Si-3p orbital. At -15˜-10 eV, the band is formed with the combination of the Si-sp with C-2s orbits. In Fig. 3(b) and (c) shows the PDOS with P substituted Si and C of the 4H-SiC, respectively. When P is substituted for Si, within -17˜-10 eV, two P-3s peaks appeared. Currently, the VCM was hybrid by the P-3p state, Si-3p state and the C-2p state, which increases the density of electron states in the VCM. The high energy segment of the P 3p state forms a donor energy level in the CBM that can provide electrons. And the electrons are generated near the bottom of the CBM. Then the Fermi level enters the CBM, which can increase the conductivity of 4H-SiC.

Fig. 3 shows the doped system works efficiently in the photoelectric conversion process. The doping system reduce the band gap and the transport time of carriers.

Measurement results: A monolithic optocoupler using the proposed PD which has fabricated by the 4H-SiC. When the temperature is 25°C, the operating voltage is 30V and the load resistor is 50Ω. The response time of the chip is measured in Fig. 4.

Rise time delay (b) Fall time delay

Fig. 4 *Experimental results of proposed optocoupler*

Horizontal scale: 50ns/div; vertical scale: 5V/div.

The blue waveform is the input pulse signal, and the green waveform is the output of the chip. The rise time of the photocoupler is 16ns, and the fall time is 14ns. The rising propagation delay is 205ns and the falling delay is 155ns. During the I_{ph} changed, when the temperature is 20 and 75, the variation value of $T_{PHL}$and T_{PLH} get maximum, with their value is 12ns and 10.7ns, respectively.

Compared with similar optocoupler chips on the market, the optocoupler designed in this paper also has fast response capability. The FOD8316 high-speed optocoupler produced by Fairchild Semiconductor is 250ns and 300ns; the HCPL-M701 produced by AVAGO is 10μs and the fall delay is 2μs; the high-speed optocoupler LTV824 produced by Liteon Company, its t_r and t_f are respectively 400ns and 300ns, these response times far exceed the whole chip response time of the chip designed in this paper.

Conclusion: The improved PD of the optocoupler was fabricated by the two photodiodes array using the 0.35μm 1P3M standard BCD process. The active area of each PD is 166*166μm^2 which concluded nine units. With the temperature range from -50 to 125, when the I_{ph} changed from 8μA to 25μA, the maximum variation value of the response time is 12.0ns. The proposed circuit combined the PD and the differential

TIA, and has the feature of fast and stable operation. It can be seen clearly the optocoupler can work faster than ever and it is suitable for the future of the hybrid integration optoelectronics signal processing.

Acknowledgments: This work was partly supported by the Natural Science Basic Research Program of Shaanxi (No.2021JM-460 and 2017JM6107) and the Scientific Research Program of Shaanxi Provincial Education Department (No.21JC033 and 16JK1695).

Received: xx January 2022 *Accepted:* xx March 2022

doi: 10.1049/ell2.10001

References

1. Tavernier, F., Hermans, C., Steyaert, M.: Optimised equaliser for differential cmos photodiodes, Electron Lett. 42 (2006), no. 17, 1002-1003
2. Yao, Y., Chen, H.Y., Huang, J., Yang, Y.: Low voltage and fast speed all-polymeric optocouplers, Appl Phys Lett. 90, (2007), no. 5, 053509-053509-3
3. Dong, G.F., Zheng, H.Y., Duan, L., Wang, L.D., Qiu, Y.: High-Performance Organic Optocouplers Based on a Photosensitive Interfacial C60/NPB Heterojunction, Advanced Materials. 21 (2009), no. 24, pp. 2501-2504
4. Marchlewski, A., Zimmermann, H., Jonak-Auer, I., Meinhardt, G., Wachmann, E.: Improvement of universal pin photodetectors in 0.35μm SiGe BiCMOS technology, Electron Lett. 45 (2009), no. 13, 705-706
5. Caillaud, C., Glastre, G., Lelarge, F., Brenot, R., Bellini, S., Paret, J.F., Drisse, O., Carpentier, D., Achouche, M.,:'Monolithic Integration of a Semiconductor Optical Amplifier and a High-Speed Photodiode With Low Polarization Dependence Loss, IEEE Photonics Technol Lett. 24 (2012), no. 11, 897-899
6. Nada, M., Muramoto, Y., Yokoyama, H., Ishibashi, T., Matsuzaki, H.: High-power-tolerant InAlAs avalanche photodiode for 25 Gbit/s applications, Electron Lett. 49 (2013), no. 1, 62-63
7. Ferhatiab, H., Djeffalb, F., Bendjeradb, A., Foughalia, L., Benhayab, A., Saidic, A.: Highly-detective tunable band-selective photodetector based on RF sputtered amorphous SiC thin-film: Effect of sputtering power, Journal of Alloys and Compounds. 907, (2022), no. 25,164464-164475.
8. Zhang, Y., Wang, Y.C., Wang, L., Zhu L.P., Wang, Z. L.: Highly Sensitive Photoelectric Detection and Imaging Enhanced by the Pyro-Phototronic Effect Based on a Photoinduced Dynamic Schottky Effect in 4H-SiC, Advanced Materials. 34, (2022), no. 1, 2204363-2204373.
9. Du, F. Y., Song, Q. W., Tang, X. Y., Zhang, Z.Y.L., Han, C., Zhang, C. F., Zhang, Y.M.: Demonstration of High-Performance 4H-SiC MISIM Ultraviolet Photodetector With Operation Temperature of 550 °C and High Responsivity, IEEE Transactions on Electron Devices, 68, (2021), no. 11, 5662-5665.
10. Bencherif, H., Meddoura, F., Dehimi, L., Faggio, G., Messina, G., Pezzimenti, F., Abdi, M.A., Della Corte, F.G.: Improving graphene/4H-SiC/graphene MSM UV photodetector sensitivity using interdigitated electrodes formalism and embedded gold plasmonic nanoparticles, Optics & Laser Technology, 148, (2021), no. 7, 1-9.
11. Guo, S.W., Zhao, X.L., He, Y.N., Pan, Z.J., Yang, M.C., Cai, Y.H., Fu, X.H., Zhang, L.L.: Low-Voltage and High-Gain Ultraviolet Detector Based on 4H-SiC n-p-n Bipolar Phototransistor, IEEE Transactions on Electron Devices, 68, (2021), no. 5, 2342-2346.